Centrifuge modeling on shallow foundation subjected to reverse faulting

Chung-Jung Lee[1], Y.Y. Chang[1], W.Y. Hung[1], W.C. Huang[1], and W.J. Huang[2]

[1] Department of Civil Engineering, National Central University, Jhongli District, Taoyuan City, Taiwan, ROC.
[2] Department of Applied Geology Engineering, National Central University, Jhongli District, Taoyuan City, Taiwan, ROC.

ABSTRACT

A series of centrifuge modeling on the free field and on a shallow foundation rested on the surface both subjected to reverse faulting with a dip angle of 60° at an acceleration of 80 g was conducted to evaluate the evolution of the surface deformation profile, the subsurface deformation pattern, the development of fault trace, and the soil-shallow foundation interaction. The magnitude of foundation bearing pressure and the location of foundation relative to the reverse fault rupture trace strongly affect the profiles of surface deformation, the fault rupture propagation traces, and the location of emergence of rupture line on the surface. The heavier foundation bearing pressure (87.2 kPa) is capable to divert the fault rupture traces and to stop the fault rupture traces emerging under the foundation.

Keywords: reverse faulting; shallow foundations; centrifuge modeling; surface and subsurface deformation pattern

1 INTRODUCTION

Earthquake-induced faulting would lead to deformation and distortion on both the ground surface and the subsurface soil. These two types of soil deformation involve permanent ground displacements during the complete (or near-complete) emergence of fault rupture on the ground surface. The displacement of overburden soil would induce angular distortion and lateral displacement on foundations and cause tremendous damages to manmade structures, especially if fault rupture traces emerge from the surface in urbanized areas. In the years of 1999, three major earthquakes occurred in Kocaeli, Turkey, in Düzce, Turkey, and in Chi-Chi, Taiwan (Dong, et al., 2004). The ground surface and subsurface deformations caused severe damage to buildings (Fig. 1), major infrastructure, tunnel, water and sewer utilities, electrical conduit systems, and power utilities. While several structures suffered severely damaged or even collapse, there were numerous structures those which survived with only small tilting after emergence of fault rupture and in some of cases the surface rupture was effectively diverted due to the presence of a structure.

Physical modeling studies (1 g and centrifuge modeling) were used to explore the fault-foundation interaction and to validate numerical simulation results. Bransby, et al. (2008), and Chang, et al. (2015) studied the normal and reverse fault-foundation interaction in a series of centrifuge model tests in which a dip angle of 60° were initiated through a sand layer, close to foundations. The test results reveal that the fault-foundation interaction depends on the foundation loading, the relative position of foundation to the fault trace, the width and the rigidity of foundation. The centrifuge tests in the study comprised of the free field test of reverse fault along 60° dip angle (without foundations) which was used to compared with those tests with foundations rested on for examination of interaction effects of reverse fault-foundation.

Fig. 1. Damages of building caused by reverse faulting in the 1999 Chi-Chi earthquake (Provided by W.J. Huang, NCU)

2 CENTRIFUGE MODELING ON REVERSE FAULT-FOUNDATION INTERACTION

2.1 Study problem

Fig. 2 shows the problem studied and displays the coordinate system, the geometry of overburden soil with a foundation rested on the surface, the fault rupture line in the free field (black dotted line), and the diverted fault rupture line in the case of foundation rested on the surface (red dotted line). The reverse fault with a dip angle of α relative to the horizontal propagates through an overburden soil of thickness H. Here W_o indicates the distance from the fault tip to the surface emergence point of lower-bound reverse fault rupture trace in the free field case (no foundation on the surface), while W_f is the distance from the fault tip to the surface emergence point of lower-bound fault rupture trace in the case of foundation on the surface. These two lower-bound traces can be investigated after the centrifuge tests. B and S are the breath of foundation, and the distance from right hand side of the foundation to the surface emergence

point of fault rupture trace in the free field case. The ratio of S/B indicates the foundation position relative to the surface emergence point of fault rupture trace in the free field case. For example, S/B=0 represents that the foundation is located on the hanging wall, S/B=1 represents the foundation located on the footwall, and S/B=0.69 represents that the foundation is across the surface emergence point of fault rupture trace and 69% of the foundation width is located on the footwall. The upward vertical displacement (positive) of reverse fault at the level of bedrock is denoted by vertical throw, h, and the ratio of vertical throw to the thickness of overburden soil, r (%), is defined as

$$r \ (\%) = \frac{h}{H} \times 100 \qquad (1)$$

The ratio of vertical throw increases from 0 – 25% for evaluation of fault trace propagation in the study.
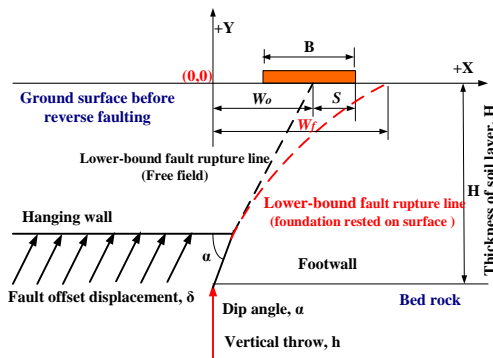
Fig. 2. Coordinate system, geometry of overburden soil layer, the foundation, and the fault tip and fault traces of reverse faulting

2.2 Testing equipment, tested sand, model foundation, and testing conditions

The experiments were undertaken on the beam centrifuge at the National Central University (NCU), Taiwan. A fault simulation container having dimensions 1000 mm × 528 mm × 675 mm (length × width × height) was designed for both the reverse fault and normal fault tests with a dip angle of 60°. A volume of 740 mm in length, 300 mm in width, and 325 mm in height was provided for the tested soil bed. A transparent acrylic window 600 mm × 281.5 mm in area was used to observe the subsurface deformation profiles during faulting. The container is capable to simulate a fault slip in a speed range of 0 – 2.5 mm/min with a displacement control mode. The maximum vertical throw reaches 55 mm. An in-flight surface profile scanner is equipped with two laser displacement transducers that installed horizontally and vertically and driven with a motor. It can travel on the centerline of the tested sand bed during faulting tests to scan the surface elevations with a sampling rate of 100 samples/sec. Fig. 3 shows the dimensions of the fault simulation container and the coordinate system used to demonstrate the testing results, as discussed in the following sections. As shown in Figs. 2 and 3, the origin of the coordinate system is the point at which the fault

tip vertically projected onto the ground surface.
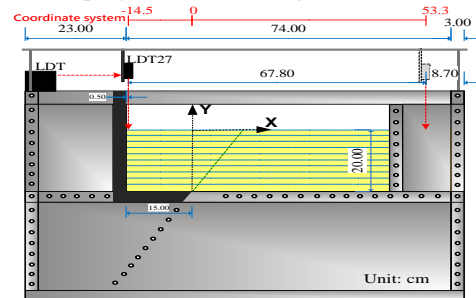
Fig. 3. Dimensions of the fault simulation container and the coordinate system used in the centrifuge experiments

Crushed quartz sand was used to prepare the uniform sand bed for all the tests conducted in this study. The fine uniform quartz sand was characterized by D_{50} = 0.149 mm. A peak friction angle of $\emptyset_{peak}$ = 41° and a dilation angle of φ = 6° was measured using a direct shear test for sand with a relative density of 70% at the normal stress = 200 kPa. The dry quartz sand was pluviated from a hopper along a regular path into the container to prepare a uniform sand deposit of relative density of approximately 70%. The pluviation process was interrupted as needed to spray a thin layer of blue dyed sand at specified elevations as marker layers in proximity to the acrylic window to allow identification of shear deformations in the subsurface, as shown in Fig.4. The sand bed 200 mm thick (H) was prepared to correspond to 16 m or 8 m on the prototype scale when tested at an acceleration of 80 *g* or of 40 *g*, respectively.

Fig. 4. Fault simulation container equipped with a surface profile scanner and sand bed with dyed sand layers before test

Table 1 lists the testing program. Here the notation of #g in the test number represents the test was conducted at #*g* (40 g or 80 g in this series), and Rtest# represents the series number of the reverse faulting test without a foundation (free field test). The later notation of -F-# after "#gRtest#" represents the case of reverse faulting test with one type of foundations (B, C type) those were placed on the surface of sand bed. Following two free field tests at an acceleration of 40 g and of 80 g, five tests were conducted to investigate the effects of bearing pressure of foundation, q, foundation breadth, B, and foundation position, S, on the fault-foundation interaction. Table 2 lists the dimensions of footings and their bearing pressures. At the testing condition of 80 g, the B-footing with a breadth of 6.44 m in prototype

simulates a bearing pressure of five-stories building; and the C-footing (B=6.44 m) simulates a bearing pressure of nine-stories building.

Table 1. Testing program

Test No.	g level	Testing condition
40gRtest21	40	Throw=50mm, Free field
80gRtest23	80	Throw=50mm, Free field
80gRtest39-F-B	80	Throw=50mm, 5f_S/B=0.69
80gRtest41-F-B	80	Throw=50mm, 5f S/B=0
80gRtest47-F-C	80	Throw=50mm, 9f S/B=0.69
80gRtest52-F-B	80	Throw=50mm, 5f_S/B=1

Table 2. Dimensions of footing and bearing pressures

Footing types	Dimensions (length x width x thickness (mm x mm x mm)	Bearing pressure at 80 g, (kPa)	Bearing pressure at 40 g, (kPa)
B	297.5 x 80.6 x9.3	54.4	27.2
C	297.5 x 80.6 x14.8	87.2	43.6

3 TEST RESULTS AND DISCUSIONS

3.1 Surface and subsurface deformation profiles in the free field

Figs. 5(a) and 5(b) display the surface deformation profiles at various throws (uplift height, s, versus horizontal distance, d, from the fault tip and the vertical throw ratio, r , ranging from 1.25% to 25%) in the cases of free field tested at the accelerations of 40 g and 80 g. As expected, the uplift height increased as the vertical throw increased. Fig. 6(a) and 6(b) show that the upper bound (black line) and the lower bound (red line) of the rupture paths at 40 g and 80 g, which was obtained by connecting the points corresponding to the minimum radii of curvature for each marker layer. These rupture paths initially extended along the dip plane and then curved out over the footwall. The zone confined within the upper and lower bounds constituted the major faulting-induced distortion zone (the shear band). The values of W_o/H ratio for 80gRtest23 and 40gRtest21 (free field tests) at r = 25% were listed in Table 3. Here W_o and U_o indicate the distance from the fault tip to the surface emergence point of lower bound and upper-bound fault rupture traces in the free field case. Table 3 summaries the positions of emergence points of the upper-bound and lower-bound rupture traces. The value of W_o, and the ratio of width of major shear distortion zone, (W_o-U_o)/H, on the surface observed from the test in the acceleration of 40 g (40gRtest21) are large than those observed from the test in the acceleration of 80 g (80gRtest23). The higher effective overburden pressure resulting from the higher testing g-level would depress the dilatancy behavior of sand layer during shearing. The higher trend of dilatancy would force the reverse fault trace declining to the footwall more.
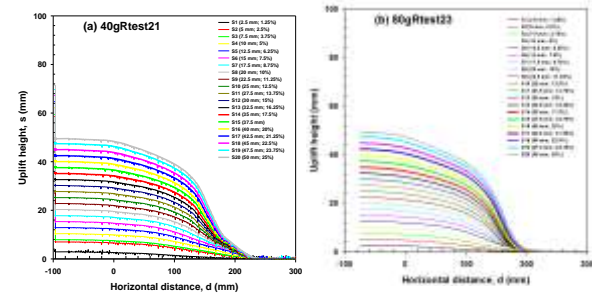
Fig. 5 Surface deformation profiles at various throws for reverse faulting: (a) 40 g ; (b) 80 g
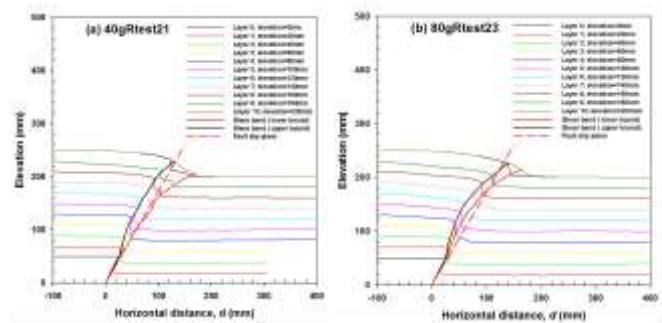
Fig. 6 Major shear-induced distortion zone after 50-mm vertical throw (r = 25%): (a) 40 g ; (b) 80 g

Table 3. Comparison of the ratios of W_f/H or W_o/H at r = 25%

Test No.	S/B	W_f or W_o (mm)	W_f/H or W_o/H
80gRtest23	-	163.88	0.82
40gRtest21	-	170.34	0.85
80gRtest39-F-B	0.69	203.4	1.02
80gRtest41-F-B	0	201.43	1.01
80gRtest52-F-B	1	160.79	0.81
80gRtest47-F-C	0.69	143.92	0.71

Table 4. Positions of emergence points of upper-bound (U) and lower-bound (W) rupture traces on the surface at r = 25%

Test No.	S/B	W_f or W_o (mm)	U_f or U_o (mm)	$(W_f -U_f)$/H or (W_o-U_o)/H
80gRtest23	-	163.88	149.87	0.07
40gRtest21	-	170.34	129.92	0.20
80gRtest39-F-B	0.69	203.4	127.69	0.38
80gRtest41-F-B	0	201.43	95.57	0.53
80gRtest52-F-B	1	160.79	143.83	0.08
80gRtest47-F-C	0.69	143.92	126.95	0.08

3.2 Surface and subsurface deformation profiles in cases of shallow foundation rested on

The major distortion zones observed at r = 25% in the tests of 80gRtest41-F-B, 80gRtest39-F-B, 80gRtest52-F-B are shown in Fig. 7(a) to 7(c). The red thin rectangular blocks on the surface as shown in Figs. 7(a) – Fig. 7(d) represent the positions of shallow foundation after reverse faulting. The developed upper bound (black line) and the lower bound (red line) of the rupture paths are shown in these figures. The B-footing with the bearing pressure of 54.4 kPa was located at the positions of S/B=0 (all the

breadth of the foundation rested on the hanging wall), S/B=0.69 (around one third of breadth of the foundation rested on the hanging wall), and S/B=1 (all the breadth of foundation rested on the footwall), respectively. Fig. 7(d) displays the major distortion zone observed at r = 25% in the test of 80gRtest47-F-C and in this test the C-footing with a bearing pressure of 87.2 kPa was located at the position of S/B=0.69.

The values of W_f/H ratio observed at r = 25% for these tests were also listed in Table 3 and Figs. 7 (a) - 7(c) for comparison of fault rupture soil-foundation structure interaction. The ratio of S/B and the magnitude of bearing pressure would strongly affect the shapes of subsurface distortion zones and the surface emergence point of reverse fault rupture trace after observing Figs. 7(a) -7(c), Table 3, and Table 4. All the breadth or the part of the breadth of the B-footing rested on the hanging wall (bearing pressure = 54.4 kPa, S/B=0 and S/B=0.69) in the tests of 80gRtest41-F-B and 80gRtest39-F-B. The stress bulb beneath the footing induced by the surface bearing pressure in these two cases forces the lower bound fault rupture traces moving more inclined to the footwall and the upper bound fault rupture traces moving more backward the hanging wall than those observed in the case of free field. These two characteristics keep the rupture traces away from penetrating into the zone beneath the footing. These two tests give the larger ratio of width of major shear distortion zone, $(W_f-U_f)/H$, observed on the surface. However, the stress bulb beneath the D-footing with the heavy bearing pressure (87.2 kPa; S/B=0.69) stopped the development of the first lower bound rupture trace and then developed the second lower bound rupture trace that finally appeared at the left edge of footing in the test of 80gRtest47-F-C as shown in Fig. 7(d). The upper bound rupture trace was close to the second lower bound rupture trace, therefore, the smaller $(W_f-U_f)/H$ was observed. All the breadth of the B-footing rested on the foot wall (S/B=1) in the test of 80gRtest52-F-B. Both the upper bound and lower fault rupture traces cannot penetrate into the stress bulb and the smaller $(W_f-U_f)/H$ was observed as well.

The existence of foundation on the ground surface would divert the fault rupture traces and change surface deformation patterns. The test results show that different ratios of S/B and the magnitude of the bearing pressure would develop different patterns of surface profiles and subsoil layer deformation. In addition, the observed top view of surface deformation shows that, while foundation position locates on the ratio of S/B=0.69 and S/B=1, the soil on the hanging wall overtopped on the shallow foundation. Consequently, the foundation (or the structure rested on) would sustain extra lateral earth pressures caused by overtopping soils and make the more tilts and the more serious damages on the structure as shown in Fig.1.
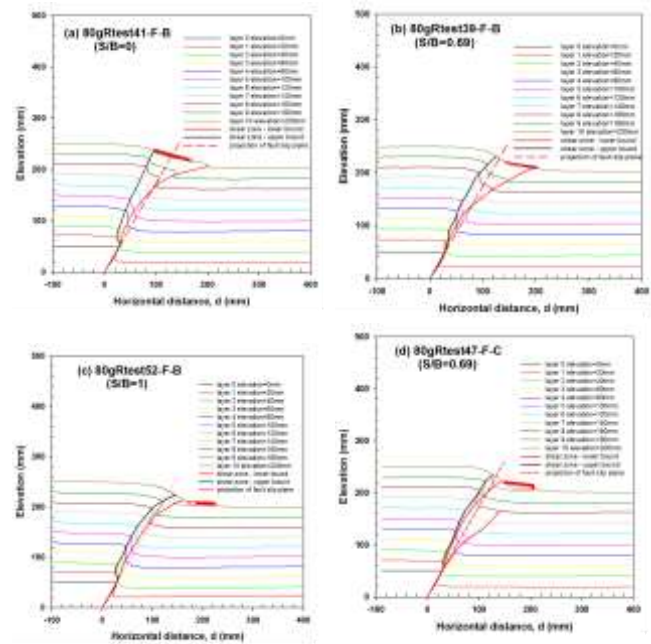
Fig. 7 Major shear-induced distortion zone after 50-mm vertical throw (r = 25%): (a) 80gRtest41-F-B ; (b) 80gRtest39-F-B ; (c) 80gRtest52-F-B ; (d) 80gRtest47-F-C

4 CONCLUSION

A series of centrifuge modeling on the free field and on a shallow foundation rested on the surface both subjected to reverse faulting with a dip angle of 60° at an acceleration of 80 g was conducted to evaluate the evolution of the surface deformation profile, the subsurface deformation pattern, the development of fault trace, and the soil-shallow foundation interaction. The stress bulb beneath the foundation keeps the rupture trace from penetrating into the zone beneath the foundation. The magnitude of foundation bearing pressure and the location of foundation strongly affect the profiles of surface deformation, the fault rupture propagation traces, and the location of emergence of rupture path on the surface. The heavier foundation bearing pressure is capable to divert the fault rupture traces and to stop the fault rupture traces emerging under the foundation.

REFERENCES

Bransby, M.F., Davies, M.C.R., EL Nahas, A., 2008. Centrifuge modelling of reverse fault-foundation interaction. Bulletin of Earthquake Engineering, 6, 607-628.

Chang, Y.Y., Lee, C.J., Huang W.C., Hung, W.Y., Huang, W.J., Lin, M.L., Lin, Y.H., 2015. Evolution of the surface deformation profile and subsurface distortion zone during reverse faulting through overburden sand. Engineering Geology, 184, 52-70

Dong, J.J., Wang, C.D., Lee, C.T., Liao, J.J., Pan, Y.W., 2003. The influence of surface ruptures on building damage in the 1999 Chi-Chi earthquakes: a case study in Fengyuan city. Engineering Geology, 71, 157-179.